Electronic Supplementary Information for

Photoactivation of triosmium dodecacarbonyl at 400 nm probed with time-resolved X-ray liquidography

Hosung Ki,[a,b] Tae Wu Kim,[c] Jiwon Moon,[d] Jungmin Kim,[a,b] Yunbeom Lee,[a,b] Jun Heo,[a,b] Kyung Hwan Kim,[e] Qingyu Kong,[f] Dmitry Khakhulin,[g] Gemma Newby,[h] Joonghan Kim,[d] Jeongho Kim,[i] Michael Wulff,[h] and Hyotcherl Ihee *[a,b]

[a]*Center for Advanced Reaction Dynamics, Institute for Basic Science, Daejeon 34141, Republic of Korea. E-mail: hyotcherl.ihee@kaist.ac.kr*
[b]*Department of Chemistry and KI for the BioCentury, Korea Advanced Institute of Science and Technology (KAIST), Daejeon 34141, Republic of Korea*
[c]*Department of Chemistry, Mokpo National University, Muan-gun, Jeollanam-do 58554, Republic of Korea*
[d]*Department of Chemistry, The Catholic University of Korea, Bucheon 14662, Republic of Korea*
[e]*Department of Chemistry, Pohang University of Science and Technology (POSTECH), Pohang 37673, Republic of Korea*
[f]*Synchrotron Soleil, L'Orme des Merisiers, Saint-Aubin, BP 48, 91192 Gif-sur-Yvette Cedex, France*
[g]*European XFEL, Holzkoppel 4, 22869 Schenefeld, Germany*
[h]*European Synchrotron Radiation Facility, BP 220, 38043 Grenoble Cedex, France*
[i]*Department of Chemistry, Inha University, Incheon 22212, Republic of Korea*

This PDF file includes:

Supplementary Methods
Supplementary Table S1
Supplementary Figs. S1-S4
Supplementary References

Supplementary Methods

Time-resolved X-ray liquidography (TRXL) experiment. The TRXL experiments were performed at beamline ID09 of the European Synchrotron Radiation Facility (ESRF). The typical laser-pump, X-ray-probe scheme was used to initiate and probe the reaction. The fundamental output from a Ti:sapphire laser (800 nm) was converted to 400 nm by frequency doubling. The optical pump pulses were spatially focused to a spot size of $170 \times 190 \ \mu m^2$, yielding a laser fluence of 2.5 mJ/mm^2. Subsequently, a time-delayed X-ray pulse was used to probe the progress of the reaction. The X-ray pulse had a duration of 100 ps with the flux of 5×10^8 photons per pulse and was quasi-monochromatic with its spectrum peaked at 18.2 keV and of 0.45 keV bandwidth. The X-ray pulse was selected from the 16-bunch filling mode of the synchrotron ring using a synchronized mechanical chopper and was focused to a spot of $100 \times 60 \ \mu m^2$ on the sample. Two-dimensional (2D) scattering patterns were collected with a Fast Readout Low Noise charge-coupled device camera (FReLoN CCD, 2048×2048, 46×46 μm^2 effective pixel size) with a sample-to-detector distance of 41 mm and an exposure time of 2 s per image. The saturated solution of $Os_3(CO)_{12}$ (Aldrich, 99.99%) in cyclohexane (< 1 mM concentration) was prepared and circulated through a high-pressure slit nozzle (0.3 mm slit, Kyburz) to form a liquid jet. The nozzle provides a stable flow of liquid and allows the refreshment of the liquid sample between subsequent laser pulses at a repetition rate of 1 kHz. The solution scattering signals were measured at various time delays between the laser and X-ray pulses: 100 ps, 316 ps, 1 ns, 3.16 ns, 10 ns. Besides, the signal at a negative time delay, S(q, -3 ns), was measured as a reference for the unexcited sample and was subtracted from the signals at positive time delays, S(q, t), to obtain the difference signals, ΔS(q, t). The obtained ΔS(q, t) was analyzed using a typical procedure, and the details of the analytic procedure are described in the following sections.

The bulk solvent response of cyclohexane was measured from a separate TRXL experiment. In the experiment, a 4 mM solution of 4-bromo-4′-(N,N-diethylamino)-azobenzene (CAS 22700-62-5, HANCHEM, 99.9%) dissolved in cyclohexane was excited at 400 nm to induce temperature jump and subsequent thermal expansion of bulk cyclohexane. 4-bromo-4′-(N,N-diethylamino)-azobenzene was used as a dye molecule because the molecule is known to efficiently dissipate the energy of incident photons to heat surrounding solvent molecules.[1-3] The difference scattering signal arising from the temperature change, $(\partial S/\partial T)_\rho$, and the density change of the bulk solvent, $(\partial S/\partial \rho)_T$ were extracted from time-resolved scattering data

measured from the laser-excited solution.

Principal component analysis. We conducted a principal component analysis (PCA) to generate species-associated difference scattering curves (SADSs) from the $\Delta S(q, t)$ measured for several time delays. First, we calculated the time-dependent concentrations of the 1st and 2nd species following the kinetic model shown in Fig. 3a. Specifically, the concentrations of the species corresponding to the kinetic model can be calculated by using the following equation.

$$c_1(t) = c_{int.,1}(t) \cdot e^{(-t/\tau)} \tag{S1}$$

$$c_2(t) = c_{int.,2}(t) \tag{S2}$$

where $c_{int.,1}$ and $c_{int.,2}$ are constants, and $\tau = 340$ ps. Then, the experimental difference scattering curves can be expressed as follows.

$$A = \begin{bmatrix} \Delta S(q,t_1) & \dots & \Delta S(q,t_{N_t}) \end{bmatrix} = \begin{bmatrix} SADS1 & SADS2 \end{bmatrix} \begin{bmatrix} c_1(t) & c_2(t) \end{bmatrix}^T = \begin{bmatrix} SADS1 & SADS2 \end{bmatrix} C^T \tag{S3}$$

where A is an $N_q \times N_t$ matrix of the experimental difference scattering curves measured at various time delays, N_q is the number of q points in the difference scattering curve at a give time delay, and N_t is the number of measured time delays.

At this stage, $c_{int.,1}$ and $c_{int.,2}$ are unknown, and thus the exact scales of the SADS1 and SADS2, which are dependent on the $c_{int.,1}$ and $c_{int.,2}$, cannot be determined. To bypass the scaling issue, the Eq. S3 was modified as follows.

$$
\begin{aligned}
A &= \begin{bmatrix} \Delta S(q,t_1) & \dots & \Delta S(q,t_{N_t}) \end{bmatrix} = \begin{bmatrix} SADS1 & SADS2 \end{bmatrix} \begin{bmatrix} c_{int.,1}(t) \cdot e^{(-t/\tau)} & c_{int.,2}(t) \end{bmatrix}^T \\
&= \begin{bmatrix} c_{int.,1}(t) \cdot SADS1 & c_{int.,2}(t) \cdot SADS2 \end{bmatrix} \begin{bmatrix} e^{(-t/\tau)} & 1 \end{bmatrix}^T \\
&= \begin{bmatrix} c_{int.,1}(t) \cdot SADS1 & c_{int.,2}(t) \cdot SADS2 \end{bmatrix} C'^T
\end{aligned}
\tag{S4}
$$

Following the Eq. S4, $c_{int.,1} \cdot SADS1$ and $c_{int.,2} \cdot SADS2$ were calculated as follows.

$$A\left(C'^{-1}\right)^T = \begin{bmatrix} c_{int.,1} \cdot SADS1 & c_{int.,2} \cdot SADS2 \end{bmatrix} C'^T \left(C'^{-1}\right)^T = \begin{bmatrix} c_{int.,1} \cdot SADS1 & c_{int.,2} \cdot SADS2 \end{bmatrix} \tag{S5}$$

The SADSs (SADS1 and SADS2) shown in Fig. 3b are $c_{int.,1} \cdot SADS1$ and $c_{int.,2} \cdot SADS2$, respectively. The identity of each intermediate, 1st and 2nd species, was determined by

comparing the $c_{\text{int.},1}$·SADS1 or $c_{\text{int.},2}$·SADS2 with the theoretically calculated difference scattering curves of candidate species for the reaction intermediates, with varying $c_{\text{int.},1}$ or $c_{\text{int.},2}$. The details are explained in the section "Identification of reaction intermediates".

Computational details of DFT calculations. Geometry optimizations of the parent species, $Os_3(CO)_{12}$, and the long-lived intermediate with a ligand vacancy at the axial position, $Os_3(CO)_{11}(ax)$, were performed using the density functional theory (DFT) with the PBE0 functional. The unrestricted formalism was used in all DFT calculations. The dhf-TZVP relativistic effective core potential (RECP) and the def2-TZVP basis sets were used for Os and other atoms (C and O), respectively. The time-dependent DFT (TDDFT) method with the same functional (TD-PBE0) and basis sets was used to calculate the excitation energies of the parent molecule, $Os_3(CO)_{12}$. The low-lying ten singlet and ten triplet states were considered in the TD-PBE0 calculations. The restricted formalism was used in the TD-PBE0 calculations. The effect of solvent (cyclohexane) was considered by using the integral equation formalism (IEF) version of the polarizable continuum model (PCM). All calculations were performed using the Gaussian09 program. The finegrid, a default grid in the Gaussian09, was used for numerical integrations in all DFT and TDDFT calculations.

Calculation of theoretical difference X-ray solution scattering curves. Theoretical difference X-ray solution scattering curves were calculated using standard X-ray solution scattering formulas.[4,5] The structural change of molecules in solution during a chemical reaction can be decomposed into three components: (i) the structural change of solute, (ii) the rearrangement of solvent cage around the solute molecules induced by the structural change of solute, and (iii) the bulk solvent response to the heat of reaction. The theoretical difference solution scattering curves, $\Delta S(q, t)_{\text{theory}}$, were calculated as a sum of the difference scattering curves calculated for each of the three components as follows:

$$
\begin{aligned}
\Delta S(q,\ t)_{\text{theory}} &= \Delta S(q,\ t)_{\text{solute}} + \Delta S(q,\ t)_{\text{solvent-cage}} + \Delta S(q,\ t)_{\text{solvent}} \\
&= \sum_k \left[\left(c_k(t) - c_k(0) \right) \cdot S_k(q)_{\text{solute}} \right] - \sum_k \left[\left(c_k(t) - c_k(0) \right) \cdot S_k(q)_{\text{solvent-cage}} \right] \quad \text{(S6)} \\
&\quad + \left(\partial S / \partial T \right)_\rho \cdot \Delta T(t) + \left(\partial S / \partial \rho \right)_T \cdot \Delta \rho(t)
\end{aligned}
$$

where k is the index of solute species, $c_k(t)$ is the concentration of kth solute species at time t,

and $S_k(q)_{\text{solute}}$ is the theoretical scattering curve of the kth solute species, and $S_k(q)_{\text{solvent-cage}}$ is the theoretical scattering curve of solvent cage around the kth solute species. The theoretical scattering curve of solute species in the ground vibrational state was calculated using the following Debye equation:

$$S_k(q)_{\text{solute}} = \sum_i^N f_i(q)^2 + \sum_i^N \sum_{j \neq i}^N f_i(q)f_j(q)\sin(qR_{ij})/qR_{ij} \qquad (S7)$$

where i and j denote the indices of atoms in the solute species, $f_i(q)$ is the atomic form factor of ith atom, and R_{ij} is the distance between i^{th} and j^{th} atoms. For the solute species in the excited vibrational state, the effect of broadening of the interatomic distance distribution due to the vibrational motion was accounted by introducing the Debye-Waller factor to Eq. S7. The modified equation is as follows:

$$S_k(q,\sigma)_{\text{solute}} = \sum_i^N f_i(q)^2 + \sum_i^N \sum_{j \neq i}^N f_i(q)f_j(q)\sin(qR_{ij})/qR_{ij} \cdot e^{-\sigma^2 q^2/2} \qquad (S8)$$

where σ^2 is the mean-squared displacement of the interatomic distances. Here, it was assumed that σ is the same regardless of i and j. Note that Eq. S8 is equivalent to Eq. S7 when $\sigma = 0$. Accordingly, Eq. S8 can be used for the calculation of the theoretical scattering curve of the solute species in the ground and excited vibrational states.

The theoretical scattering curve of the solvent cage around solute species, $S_k(q)_{\text{solvent-cage}}$, was calculated with the aid of molecular dynamics (MD) simulation. Briefly, the pair distribution functions (PDFs) were obtained using the MD snapshots obtained from MD simulation, and the theoretical scattering curves were calculated from the PDFs by using the Debye equation. The details of the MD simulation are described in the following section. The bulk response of the solvent to the heat of reaction, $\Delta S(q, t)_{\text{solvent}}$, was calculated as a linear combination of the bulk solvent responses of cyclohexane, $(\partial S/\partial T)_\rho$, and $(\partial S/\partial \rho)_T$, obtained from a separate experiment as described in the section "Time-resolved X-ray liquidography (TRXL) experiment". The detailed protocol for calculating the theoretical difference scattering curves is described in our previous publications.[6,7]

Details of the theoretical calculation of scattering contribution from the solvent-solute cage. To consider the rearrangement of the solvent cage around the solute molecules induced

by the structural change of solute, that is, $\Delta S(q, t)_{\text{solvent-cage}}$ mentioned in the previous section, we implemented MD simulation combined with DFT calculation. Prior to starting the MD simulation, the atomic charges of individual atoms in the osmium complex were characterized by applying the natural population analysis (NPA) to the result of DFT calculations. These charges on individual atoms were kept fixed during the simulation. All the MD simulations were performed with the GROMACS 4.5.5 package,[8] employing OPLS all-atom force field[9] and atomic charge values from the NPA in combination with the Berendsen thermostat[10]. The periodic boundary conditions were used with a cubic box of 310.01 nm^3 containing one solute molecule embedded in 1720 cyclohexane molecules. The cyclohexane molecule was optimized by DFT calculations and was used for the description of the solvent (explicit solvent model). The simulation box was equilibrated for 2 ps at 293 K. The PDFs were calculated from the analysis of the MD trajectory and used for the calculation of the scattering intensity.

Identification of reaction intermediates. The identities of the intermediates involved in the reaction were determined by comparing the SADSs obtained from the PCA with the theoretical difference scattering curves calculated from candidate intermediates. We note that, in general, the bond length obtained from DFT optimization is slightly longer than the value determined from the solution scattering experiment.[11-13] Considering this trend of overestimation by DFT calculation, the theoretical difference curves were calculated using Eq. S8 with the structures that are slightly contracted from the DFT-optimized molecular structures. The optimized contraction factors for $Os_3(CO)_{12}$ and $Os_3(CO)_{11}(ax)$ are 0.970 (97.0 %) and 0.958 (95.8 %), respectively.

The following equation was used for the calculation of the theoretical difference scattering curve.

$$\Delta S_{\text{int.}}(q)_{\text{solute}} = \sum_{k}^{\text{int.}} S_k(q, \sigma_k)_{\text{solute}} - \sum_{k}^{\text{react.}} S_k(q, \sigma_k)_{\text{solute}} \tag{S9}$$

where $S_k(q, \sigma_k)_{\text{solute}}$ is the theoretical difference scattering curve corresponding to the kth solute species calculated by using Eq. S8 and the terms 'int.' and 'react.' denote intermediates and reactants, respectively. Specifically, the 'int.' and 'react.' at the top of the sigma symbols indicate the sum over the intermediate species and the reactant species, respectively. For

example, for the reaction $Os_3(CO)_{12} \rightarrow Os_3(CO)_{11}(ax) + CO$, $\sum\limits_{k}^{int.}$ denotes the sum for the two

species corresponding to the intermediates, $Os_3(CO)_{11}(ax)$ and CO, and $\sum\limits_{k}^{react.}$ denotes the term

calculated for the single reactant species, $Os_3(CO)_{12}$. Note that only the scattering contribution from the solute molecules was considered in the calculation of the theoretical difference scattering curves. For the comparison with the experimental SADSs, the theoretical scattering curve of a reaction intermediate was multiplied by two constants, (1) the concentration of the intermediate and (2) the scaling factor between the experimental data and the theoretical curve, as follows:

$$\Delta S_{int.}(q)_{solute,scaled} = c_{int.} \cdot \kappa \cdot \Delta S_{int.}(q)_{solute}$$
$$= c_{int.} \cdot \kappa \cdot (\sum\limits_{k}^{int.} S_k(q,\sigma_k)_{solute} - \sum\limits_{k}^{react.} S_k(q,\sigma_k)_{solute}) \tag{S10}$$

where $c_{int.}$ is the concentration of the reaction intermediate, and κ is the scaling factor between the experimental data and theoretically calculated scattering curves. Since the concentration of the reaction intermediate, $c_{int.}$, is unknown, the value is allowed to vary freely. When comparing $\Delta S_{int.}(q)_{solute, scaled}$ calculated for the vibrationally hot $Os_3(CO)_{12}$ or $Os_3(CO)_{11}(ax)$, the optimal $c_{int.}$ could not be accurately determined because the values strongly correlate with σ^2, the mean-squared displacement of the interatomic distances. Here, instead of optimizing both σ^2 and $c_{int.}$, we determined the $c_{int.}$ assuming that $\sigma^2 = 0.01 \text{ Å}^2$.

The comparison in Fig. 3b shows that the vibrationally hot $Os_3(CO)_{12}$, i.e., hot $Os_3(CO)_{12}$, and $Os_3(CO)_{11}(ax) + CO$ matches the SADS1 and SADS2, respectively. The theoretical curve corresponding to the MMBC intermediate does not show a reasonable agreement with either SADS1 or SADS2, indicating that the formation of the MMBC intermediate is not supported by the TRXL data.

Structural refinement. To refine the DFT-optimized structures of intermediates and $Os_3(CO)_{12}$, the experimental data were fitted using linear combination fitting (LCF). All three contributions from solute, cage, and solvent were considered using the following equation:

$$\Delta S(q,\ t)_{\text{theory}} = \Delta S(q,\ t)_{\text{solute}} + \Delta S(q,\ t)_{\text{solvent}} + \Delta S(q,\ t)_{\text{solute-solvent}}$$

$$= \Delta S(q,\ t)_{\text{solute}} + \left(\partial S/\partial T\right)_{\rho} \cdot \Delta T(t) + \left(\partial S/\partial \rho\right)_{T} \cdot \Delta \rho(t) + \Delta S(q,\ t)_{\text{solute-solvent}}$$

$$= c_{\text{int.,1}} \cdot \kappa \cdot \left(\Delta S_{\text{int.,1}}(q)_{\text{solute}} + \Delta S_{\text{int.,1}}(q)_{\text{solute-solvent}}\right) \qquad \text{(S11)}$$

$$+ c_{\text{int.,2}} \cdot \kappa \cdot \left(\Delta S_{\text{int.,2}}(q)_{\text{solute}} + \Delta S_{\text{int.,2}}(q)_{\text{solute-solvent}}\right)$$

$$+ \Delta T(t) \cdot \left(\partial S/\partial T\right)_{\rho} + \Delta \rho(t) \cdot \left(\partial S/\partial \rho\right)_{T}$$

where $\Delta S_{\text{int.,1}}(q,\ t)_{\text{solute}}$ and $\Delta S_{\text{int.,2}}(q,\ t)_{\text{solute}}$ are the difference solute terms corresponding to the two intermediates, $Os_3(CO)_{11}(ax) + CO$ and hot $Os_3(CO)_{12}$, respectively, calculated using Eq. S9, $c_{\text{int.,1}}(t)$ and $c_{\text{int.,2}}(t)$ are the concentrations of the two intermediates at time t, and $\Delta S_{\text{int.,1}}(q)_{\text{solvent-solvent}}$ and $\Delta S_{\text{int.,2}}(q)_{\text{solvent-solvent}}$ are the cage terms calculated from the pair distribution functions that were obtained from MD simulations. Here, a direct method (LU decomposition[14]) was used to obtain the exact solution of the LCF. To refine the molecular structures of $Os_3(CO)_{11}(ax)$, hot $Os_3(CO)_{12}$, and $Os_3(CO)_{12}$, we iteratively performed the LCF with changing the molecular structures to minimize χ^2, which is defined as follows:

$$\chi^2 = \sum_{j}^{N_t} \sum_{i}^{N_q} [(\Delta S(q_i,\ t_j) - \Delta S(q_i,\ t_j)_{theory})/\sigma(q_i, t_j)]^2 \qquad \text{(S12)}$$

where N_t is the number of measured time delays, N_q is the number of measured q-points, and $\sigma(q_i, t_j)$ is the standard error of the mean of $\Delta S(q_i, t_j)$. The molecular structure of hot $Os_3(CO)_{12}$ was assumed to be identical to $Os_3(CO)_{12}$ in its vibrational ground state. Two independent parameters for each molecule were used for the iterative structural refinement. Among the two parameters, one was used to scale the size of the entire molecule, and the other was used to scale the Os–Os distances. The two parameters were allowed to vary up to ± 10 % from the unity. While the second parameter affects only to Os–Os distances, the first parameter allows to modify the distances other than Os–Os such as Os–C and Os–O as well. The time-dependent concentrations, $c_{\text{int. 1}}(t)$ and $c_{\text{int. 2}}(t)$, obtained from the LCF are shown in Fig. 3d as scatter plots together with their theoretical fits based on the kinetic model shown in Fig. 3a as dashed lines. The hydrodynamic response of solvent, i.e., $\Delta T(t)$ and $\Delta \rho(t)$, obtained from the LCF are displayed in Fig. S4.

Supplementary Table

Supplementary Table S1. Comparison of DFT-optimized structures of reactants and reaction intermediates and the best-fit structures determined with the TRXL data. The bond lengths between osmium atoms in each structure are listed. Errors for the best-fit structures obtained from the global fit analysis of the TRXL data are shown in parentheses.

	Os–Os bond length (Å)		Difference	
	DFT optimized	best fit	absolute (Å)[a]	ratio (%)[b]
$Os_3(CO)_{12}$	2.917	2.829 ($\pm$ 0.012)	0.088	3.0
	2.927*	2.839* ($\pm$ 0.012)	0.088	
$Os_3(CO)_{11}(ax)$	2.764*	2.648* ($\pm$ 0.011)	0.116	4.2
	2.936	2.812 ($\pm$ 0.012)	0.124	

[a]Bond length (DFT optimized) - bond length (best fit).

[b](bond length (DFT optimized) - bond length (best fit)) / bond length (DFT optimized) × 100.

*Two bonds having the same bond length.
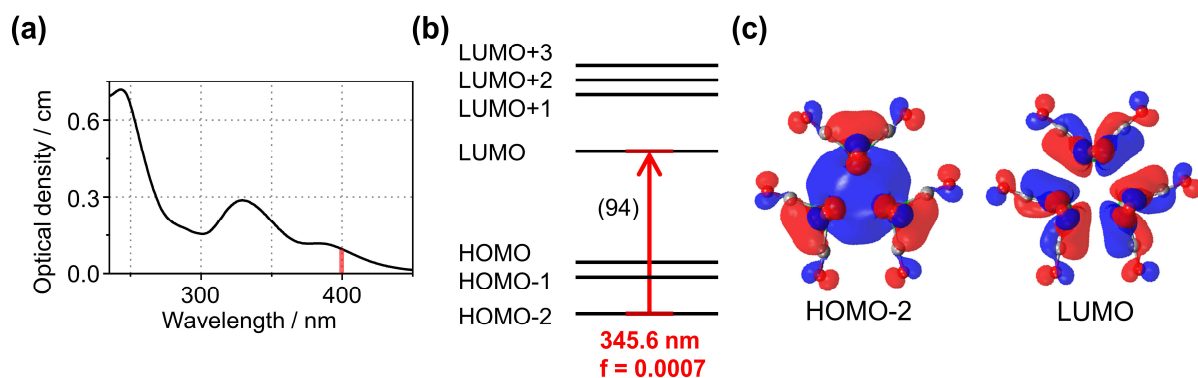
Supplementary Figures

(a)

(b)

LUMO+3
LUMO+2
LUMO+1

LUMO

(94)

HOMO
HOMO-1

HOMO-2

345.6 nm
f = 0.0007

(c)

HOMO-2   LUMO

Fig. S1 (a) Absorption spectrum of 40 μM solution of $Os_3(CO)_{12}$ dissolved in cyclohexane. The red vertical line indicates the excitation wavelength (400 nm) used in this study. (b) The characters of the electronic transition resonant with 400 nm excitation (red arrow). The characters of the electronic transitions were calculated using TDDFT method (TD-PBE0) and the details of the TDDFT calculations are described in the section "Computational details of DFT calculations". The oscillator strength of this transition was estimated to be quite small (f = 0.0007), probably because the spin-orbit coupling was not considered in the TDDFT calculation. (c) The molecular orbitals involved in the electronic transitions initiated by the 400 nm excitation. The molecular orbitals were visualized using the Chemissian program[15].
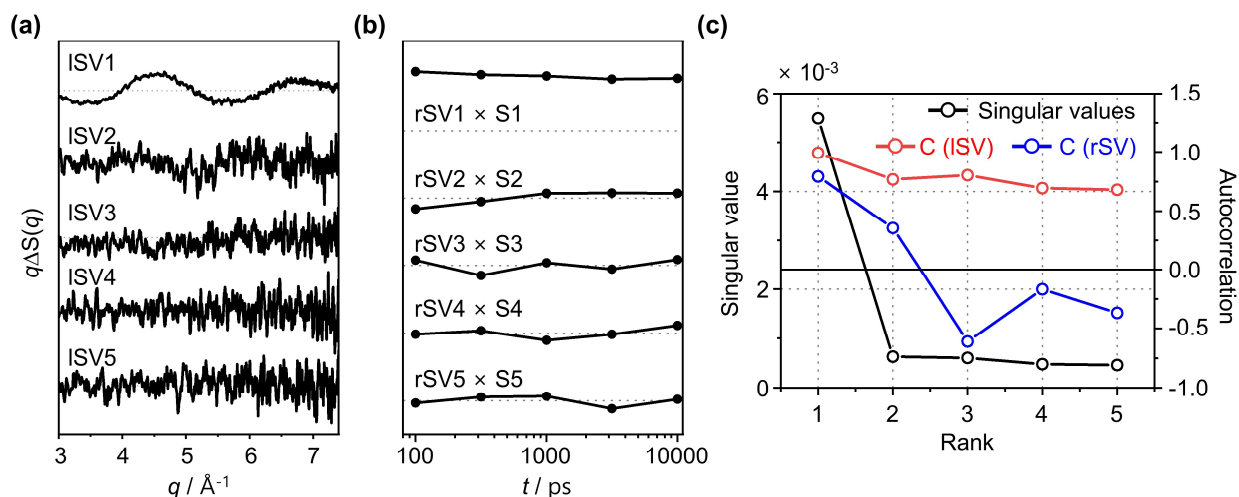
(a)

ISV1
ISV2
ISV3
ISV4
ISV5

(b)

rSV1 × S1
rSV2 × S2
rSV3 × S3
rSV4 × S4
rSV5 × S5

(c)

Fig. S2 SVD analysis of TRXL data for $Os_3(CO)_{12}$. Only the high-q region ($q > 3$ Å^{-1}) where the contribution of the solvent term is negligible (See Fig. S3) was subjected to the SVD analysis. (a-b) The first five left (a) and right (b) singular vectors (lSVs and rSVs) of TRXL data. The rSVs are weighted by the corresponding singular values. (c) The singular values, and the autocorrelation values (C) for rSVs and lSVs. The singular values and autocorrelation values, together with the signal-to-noise ratio of the lSVs, indicate that there are two signal components contributing significantly to the TRXL data.
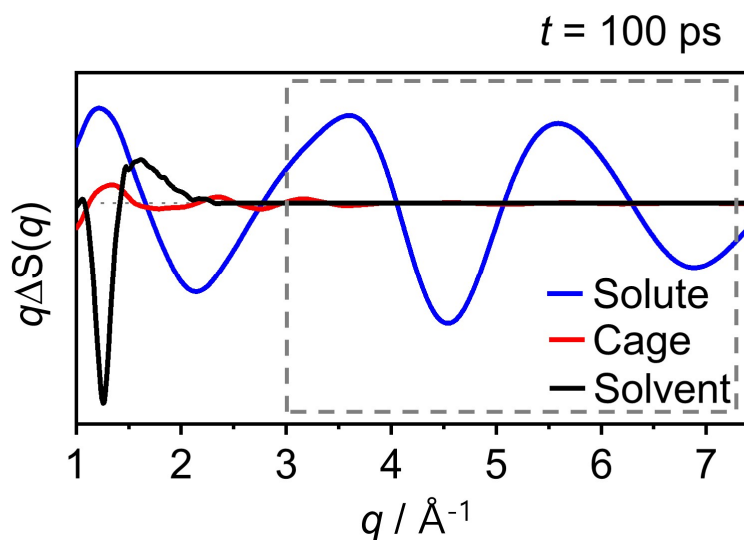
Fig. S3 Comparison of the solute (blue), cage (red), and solvent (black) contributions to the experimental curve for 100 ps time delay. The contribution from solvent and cage is negligible in a high-q region ($q > 3$ Å^{-1}).
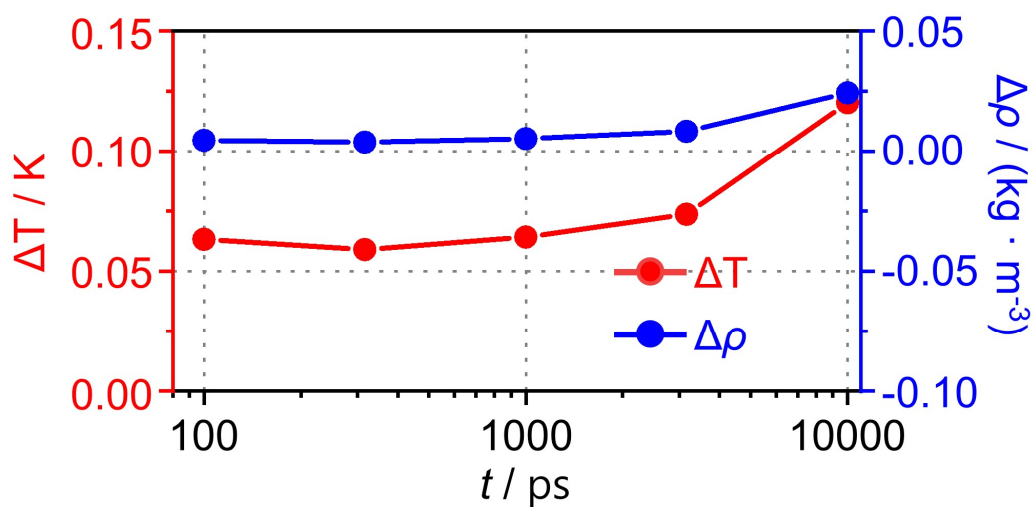

Fig. S4 Time-dependent changes of the temperature and density of the solvent induced by photoreaction of $Os_3(CO)_{12}$. The profiles were obtained by using linear combination fitting (LCF) of $\Delta S(q, t)$ for each time delay. A direct method was used to obtain the exact solution of linear combination fitting without iteration. The details of the LCF are described in the section "Structural refinement" in ESI.

Supplementary References

1. K. S. Kjær, T. B. van Driel, J. Kehres, K. Haldrup, D. Khakhulin, K. Bechgaard, M. Cammarata, M. Wulff, T. J. Sørensen and M. M. Nielsen, *Phys. Chem. Chem. Phys.*, 2013, **15**, 15003-15016.

2. M. R. Panman, E. Biasin, O. Berntsson, M. Hermann, S. Niebling, A. J. Hughes, J. Kübel, K. Atkovska, E. Gustavsson, A. Nimmrich, A. O. Dohn, M. Laursen, D. B. Zederkof, A. Honarfar, K. Tono, T. Katayama, S. Owada, T. B. van Driel, K. Kjaer, M. M. Nielsen, J. Davidsson, J. Uhlig, K. Haldrup, J. S. Hub and S. Westenhoff, *Phys. Rev. Lett.*, 2020, **125**, 226001.

3. H. Ki, S. Choi, J. Kim, E. H. Choi, S. Lee, Y. Lee, K. Yoon, C. W. Ahn, D. S. Ahn, J. H. Lee, J. Park, I. Eom, M. Kim, S. H. Chun, J. Kim, H. Ihee and J. Kim, *J. Am. Chem. Soc.*, 2021, **143**, 14261-14273.

4. H. Ihee, M. Lorenc, T. K. Kim, Q. Y. Kong, M. Cammarata, J. H. Lee, S. Bratos and M. Wulff, *Science*, 2005, **309**, 1223-1227.

5. K. H. Kim, H. Ki, J. H. Lee, S. Park, Q. Kong, J. Kim, J. Kim, M. Wulff and H. Ihee, *Phys. Chem. Chem. Phys.*, 2015, **17**, 8633-8637.

6. T. K. Kim, M. Lorenc, J. H. Lee, M. Russo, J. Kim, M. Cammarata, Q. Y. Kong, S. Noel, A. Plech, M. Wulff and H. Ihee, *Proc. Natl. Acad. Sci. USA*, 2006, **103**, 9410-9415.

7. K. H. Kim, J. G. Kim, S. Nozawa, T. Sato, K. Y. Oang, T. Kim, H. Ki, J. Jo, S. Park, C. Song, T. Sato, K. Ogawa, T. Togashi, K. Tono, M. Yabashi, T. Ishikawa, J. Kim, R. Ryoo, J. Kim, H. Ihee and S. Adachi, *Nature*, 2015, **518**, 385–389.

8. D. Van der Spoel, E. Lindahl, B. Hess, G. Groenhof, A. E. Mark and H. J. C. Berendsen, *J. Comput. Chem.*, 2005, **26**, 1701-1718.

9. W. L. Jorgensen, D. S. Maxwell and J. TiradoRives, *J. Am. Chem. Soc.*, 1996, **118**, 11225-11236.

10. H. J. C. Berendsen, J. P. M. Postma, W. F. Vangunsteren, A. Dinola and J. R. Haak, *J. Chem. Phys.*, 1984, **81**, 3684-3690.

11. Q. Kong, J. H. Lee, A. Plech, M. Wulff, H. Ihee and M. H. J. Koch, *Angew. Chem. Int. Ed.*, 2008, **47**, 5550-5553.

12. P. Hirva, M. Haukka, M. Jakonen and M. A. Moreno, *J. Mol. Model.*, 2008, **14**, 171-181.

13. Y. Minenkov, A. Singstad, G. Occhipinti and V. R. Jensen, *Dalton Trans.*, 2012, **41**, 5526-5541.

14. A. Schwarzenbergczerny, *Astron. Astrophys. Sup.*, 1995, **110**, 405-410.

15. S. Leonid, Chemissian, a computer program to analyse and visualise quantumchemical calculations (Version 4.43), http://www.chemissian.com/, 2005-2016.